Dynamic Behavior of Missiles Released from a Helicopter with Downwash Effect

COSTERG Fabien, DENG Shuanghou, QIAO Hongyu*

College of Aerospace Engineering, Nanjing University of Aeronautics and Astronautics, Nanjing 210016, P. R. China

(Received 6 July 2025; revised 15 November 2025; accepted 1 December 2025)

Abstract: This study is dedicated to numerically investigate the dynamic behavior of a missile released from a helicopter under the influence of downwash from the rotating rotors using AGM-114 Hellfire and UH-60 as the testcase. Simulations are conducted using unsteady Reynolds-averaged Navier-Stokes (URANS) with shear stress transport (SST) k-ω turbulence model, incorporating six-degree-of-freedom (6-DOF) motion and overset grid. Two releasing scenarios, viz., hover and forward flight, are analyzed under varying missile launch thrust and helicopter forward flight speed. Results reveal that the rotor downwash significantly affects the stability of the missile, particularly during hovering case, where low thrust prolongs wake interaction. In forward flight, the increased airspeed can in principle reduce wake influence but introduces asymmetrical aerodynamic effects on the trajectory of the missile. The findings offer guidance for missile release and launch planning in rotorcraft operations.

Key words: helicopter rotor wake; downwash effect; six-degree-of-freedom (6-DOF) model; unsteady Reynolds-averaged Navier-Stokes (URANS); release problems

CLC number: V211.3 **Document code:** A **Article ID:** 1005-1120(2026)01-0027-13

0 Introduction

The contemporary development of rotary-wing aircraft has significantly broadened the scope of their operational applications. Among others, defense usage includes missile carrying and release[1]. Safe and accurate release of air-launched munitions from a helicopter remains a significant challenge due to the complex aerodynamic environment generated by the main rotor. Indeed, the airflow generated by the helicopter's rotor is among the most complex flow[2] and alters the airflow approaching the blades by causing sporadic fluctuations in lift and increase drag[3-4] which contributes to the rotor efficiency and stability. The highly turbulent airflow is mainly generated due to the blade-vortex interaction (BVI) which is the result of the interaction between the rotor blades and the tip vortices (TVs)[5-6] created by the precedent blade, as illustrated in Fig.1[6].

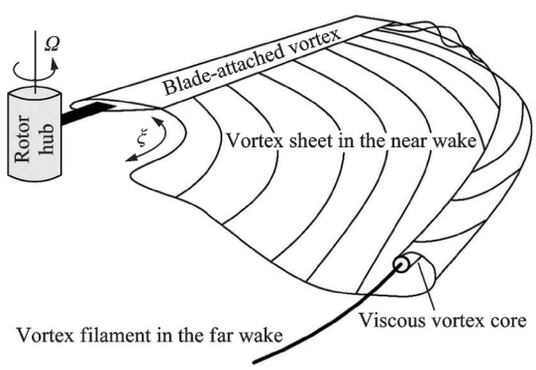

Fig.1 Sketch of the rotor wake generation[6]

Weapon release accuracy also asks to understand the release process and the interactions with the rotor wake in the near-launch period. Within this context, the investigation of external projectiles associated with fixed-wing aircraft has received limited attention in the existing literature. Shanks et al.[7] made use of a three-dimensional dynamic structured

*Corresponding author, E-mail address: shuanghoudeng@nuaa.edu.cn.

How to cite this article: COSTERG Fabien, DENG Shuanghou, QIAO Hongyu. Dynamic behavior of missiles released from a helicopter with downwash effect[J]. Transactions of Nanjing University of Aeronautics and Astronautics, 2026, 43(1): 27-39.

http://dx.doi.org/10.16356/j.1005-1120.2026.01.003

overset mesh to simulate aerodynamics and missile dynamics of a finless missile separating from a wing in a transonic flow. This study used a powered missile to showcase the effect of a missile and its plume on the wing. Cavallo et al.[8] in their case simulated the rocket stage separation and missile launched from a fighter jet wing. In their research, they used a three-dimensional unstructured mesh Navier-Stockes flow solver and coupled with a parallel moving mesh technique. In addition, the use of an adaptive mesh refinement highly helped to improve the accuracy of the results obtained. For the rotor-wing platforms, a study of the effect of the main rotor on an air-launched rocket was experimentally conducted in Ref.[9]. In their experiment, an AH-1G helicopter model operated in low-speed forward flight scenario. Thus, they measured the rotor wake induced in the launched rockets trajectory. The trajectory of a penguin missile released from an SH-2G helicopter was conducted in Ref.[10]. They used a vortex wake model to calculate the rotor wake's generated interference velocity and a panel technique for the fuselage airflow interference. Subsequently, the measured flowfield data were converted to the interference coefficient and incorporated into a six-degree-of-freedom (6-DOF) trajectory simulation system. In this study, the simulations have been completed for different weather and operating conditions. More recently, Lee et al.[11] conducted a study in which a three-dimensional unstructured overset mesh approach was used to simulate air-launched rockets in a free flight from a full helicopter configuration. To characterize the trajectory of the air-launched rocket, a 6-DOF dynamic equation solver was also used. The simulation showed the temperature gradient along the helicopter fuselage, the path of the rocket and the perturbation caused by the rotor wake. Additionally, Zhou et al.[12] used the same technique to simulate the effects of the rotor wake on a free-falling rocket and its impact on its accuracy and release safety. It showed that the rotor's downwash flow induced perturbation in the trajectory and could be effective as soon as the release occurs. In the UH-60 Black Hawk case, Gong et al.[13] examined the downwash induced by the rotor using the actuator disk model and compared the effect on a released Sierra bullet and a Hydra70 rocket. The trajectory and range of both were displayed and it was acknowledged that the downwash effect was higher on the Hydra rocket than for the bullet. However, it did not consider effects that external winds and air perturbation could have on the rotor wake and the trajectory and range of the rocket.

While previous studies have offered useful observations regarding the effect of rotor downwash on rocket trajectories, a more detailed numerical investigation is still required, as the rotor-generated flow field is highly complex and strongly dependent on the test configuration. In the present study, the dynamic behavior of the AGM-114 Hellfire missile released from the UH-60 Black Hawk helicopter is investigated using high-fidelity computational fluid dynamics (CFD). A particular focus is placed on quantifying the influence of rotor-induced downwash on missile behavior. The simulation framework relies on the unsteady Reynolds-averaged Navier-Stokes (URANS) equations coupled with a 6-DOF solver. The shear stress transport (SST) k-ω turbulence model is employed to capture both the boundary layer characteristics and the detached flow structures, providing a balance between computational cost and accuracy.

1 Methodology

1.1 Model description

The computational model used in this study comprises a simplified representation of the UH-60 Black Hawk helicopter and an AGM-114 Hellfire missile. The model got simplified by removing the tail rotor. Crozon et al.[14] used a model without tail rotor to simulate helicopter behavior in a ship air wake. Also, Wadcock et al.[15] simulated the air wake of a helicopter and modelled the tail rotor as a simple uniform pressure disk which reduces its precision and indicates a lower interest or application with the main rotor downwash. At the same time,

the missile has been only present on one side of the helicopter. Okamoto et al.[16] and Ryu et al.[17] only considered the release of missile on one side of the helicopter. In the simulation configuration, the Hellfire missile is only present on the left-hand side of the helicopter and is mounted beneath the helicopter fuselage in a typical launch position (Fig.2). These modifications and simplification are justified since the study primarily focuses on the interaction between the main rotor downwash and the missile trajectory during the early release phase.

Fig.2 Simplified UH-60 Black Hawk helicopter model

1.1.1 Main rotor specifications of UH-60

The main rotor system of the helicopter is modeled with a 4-bladed rotor, consistent with the actual UH-60 platform. During the simulation, the rotor operates in hover or high-speed forward flight, generating the downwash environment that interacts with the missile. The key rotor parameters are summarized in Table 1[18]. The blades are treated as rigid bodies with a constant collective and cyclic pitch.

Table 1 UH-60 main rotor parameters[18]

Parameter	Value
Number of blades	4
Rotor diameter/m	16.36
Blade root chord/m	0.53
Blade tip chord/m	0.26
Equivalent blade twist/(°)	−18 (linear)
Rotation rate Ω/(r·min^{-1})	258
Airfoil profile	SC1095/SC1094 R8

1.1.2 AGM-114 Hellfire missile specifications

The AGM-114 Hellfire missile is modeled as a rigid body with its aerodynamic control surface in a fixed position (non-actuated). The specifications of the missile are listed in Table 2[19] and the model can be seen in Fig.3, respectively. During the simulation, the missile is initially mounted in a fixed position and released to allow it to respond freely to aerodynamic and gravitational forces through the use of a coupled 6-DOF solver.

Table 2 AGM-114 Hellfire key parameters[19]

Parameter	Value
Length/m	1.63
Diameter/m	0.18
Launch mass/kg	approximately 45
Center of gravity position/m	approximately 0.7 (from nose)
Fin disposition	Crucifix shape

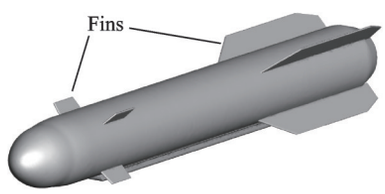

Fig.3 AGM-114 Hellfire model used in the simulation

1.1.3 Mesh configuration

Numerical simulation utilized an unstructured overset mesh grid[20] approach to accommodate the complex interactions among the rotating blades, helicopter fuselage, and moving missile, allowing each major component to be meshed independently and overlapped within the computational domain[21-22]. All component meshes are generated using polyhedral cells, which is chosen for their ability to conform to complex geometries, resolve flow gradients efficiently and offer improved convergence behavior and reduced cell count for a given level of accuracy compared to tetrahedral grids.

The overset approach ensures accurate interpolation between overlapping grids and allows smooth motion of rotating and translating bodies, which is essential to model blade motion as well as the 6-DOF motion of the missile in the early separation stage[23-24]. Thus here, each rotor blade as well as the missile is given a dedicated mesh domain that rotates about the rotor axis using a body-fitted overset grid. The helicopter fuselage, as considered fixed in the domain is discretized with its own static grid.

To ensure smoother and more accurate treatment of the different flow physics, different refinement zones have been used (Fig.4):

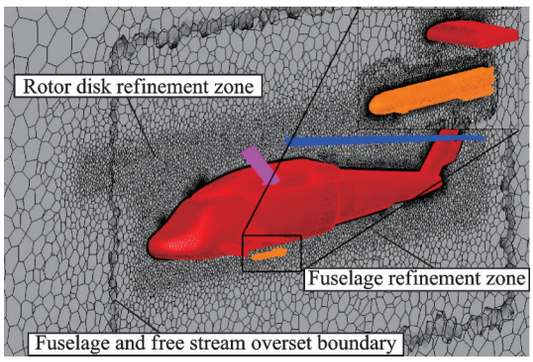

Fig.4 Mesh system of the computational model

(1) Along the rotor disk, a local mesh refinement is applied to accurately capture the tip vortices and downwash effects.

(2) The region beneath the helicopter, where the missile is released, is finely refined to resolve the rapid changes in pressure and velocity fields during separation.

(3) A refinement zone is included near the fuselage surface to capture boundary layer effects and wake formation.

1.2 Numerical methodology and setup

This section describes the numerical framework used to simulate the dynamic release of a missile from a helicopter in the presence of rotor downwash. The simulations were carried out using the CFD software Star CCM+, which provides integrated support for unsteady flow solvers, overset mesh handling, turbulence modeling, and 6-DOF rigid body motion.

1.2.1 Governing equation

Star CCM+ solves the compressible URANS equations in a finite volume framework. These equations govern the conservation of mass, momentum, and energy in the flow-field and are expressed as follows.

Continuity equation is shown as

$$\frac{\partial \rho}{\partial t}+\nabla\cdot(\rho \boldsymbol{u})=0 \tag{1}$$

Momentum equation is shown as

$$\frac{\partial \rho \boldsymbol{u}}{\partial t}+\nabla\cdot(\rho \boldsymbol{u}\otimes\boldsymbol{u})=-\nabla p+\nabla\cdot\tau+\rho g \tag{2}$$

Energy equation is shown as

$$\frac{\partial \rho E}{\partial t}+\nabla\cdot[(\rho E+p)\boldsymbol{u}]=\nabla\cdot(\tau\cdot\boldsymbol{u}+q) \tag{3}$$

where ρ is the density, $\boldsymbol{u}$ the freestream velocity vector, p the static pressure, τ the viscous stress tensor, q the heat flux, and E the total energy per unit of mass.

Turbulence effects are modeled using the SST k-ω model introduced by Menter[25-26], which offers robust performance for complex flows involving separation, vortex shedding, and adverse pressure gradients, They are condition characteristics of rotorcraft downwash and missile release.

1.2.2 Trajectory prediction by CFD-6-DOF

The interaction between the aerodynamic environment and the missile's motion is captured through the CFD-6-DOF rigid body coupling module in Star CCM+. This feature enables dynamic simulation of the missile's free-flight behavior following release, accounting for both translational and rotational motions in real time. Thus, it solves the following equations.

Translational dynamics is shown as

$$m\frac{\mathrm{d}\boldsymbol{V}}{\mathrm{d}t}=F_{\text{aero}}+mg \tag{4}$$

Rotational dynamics is shown as

$$I\frac{\mathrm{d}\boldsymbol{\omega}}{\mathrm{d}t}+\boldsymbol{\omega}\times(I\boldsymbol{\omega})=\boldsymbol{M}_{\text{aero}} \tag{5}$$

where m is the missile mass, $\boldsymbol{V}$ the missile velocity vector, and $\boldsymbol{\omega}$ the angular velocity vector; F_{aero} and $\boldsymbol{M}_{\text{aero}}$ are respectively the aerodynamic force and moment vector computed at each physical time step; and I is the missile's inertia tensor.

The missile is treated as an active rigid body with a constant unidirectional acceleration positioned in its nozzle and running along its local X-axis. The updated position and orientation of the missile are communicated to the CFD solver using overset mesh interpolation, enabling seamless tracking of the missile's movement through the rotor wake field.

1.3 Validation

To ensure the reliability of the present method for predicting the dynamic behavior of a store coupled with a 6-DOF equation of motion and the induced downwash generated by the helicopter main rotor, two different validation calculations were carried out. To validate the rotor downwash predic-

tion, the flow around a rotor-fuselage configuration was calculated. Then, for the trajectory simulation, an external store released from a fixed wing was simulated.

1.3.1 Flow downwash prediction validation

The first validation case is targeting to validate the flow downwash prediction capability using the rotor body interaction (ROBIN) model[27-29]. For that, an unsteady flow calculation around model was made. The experimental work that will serve as a comparison was performed in the Langley Subsonic Tunnel with the model rotor rotated at 2 000 r/min and has an advance ratio $\mu = 0.15$. The model is composed of a background domain, a fuselage and blades, as seen in Fig.5. The background is composed of 16 million hexahedral cells, and the fuselage and each blade have 2 million and 0.7 million cells, respectively.

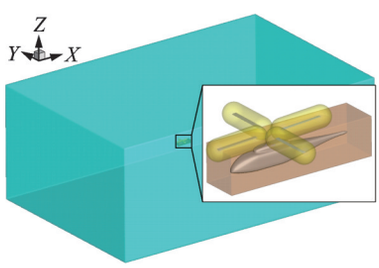

Fig.5 ROBIN case geometry

Fig.6(a) shows the comparison of time-averaged pressure coefficient C_p along the center line of the fuselage for the experimental case and the present validation case with the URANS solver. Fig.6(b) shows the comparison of C_p distribution along the longitudinal center line of the fuselage for an azimuthal position of the rotor of $\psi = 0°$. The data present close results between the two different tests and enlighten the capacity of reproducing conditions near real behavior. This helps to validate the utilization of the URANS solver of Star CCM+ to follow the study of this article.

1.3.2 Releasing trajectory validation

To validate the missile release process and the 6-DOF solver capability, the present method was applied to the EGLIN test model which is composed of a 45° delta fixed wing mounted of a pylon and releasing a store by the use of ejector. The

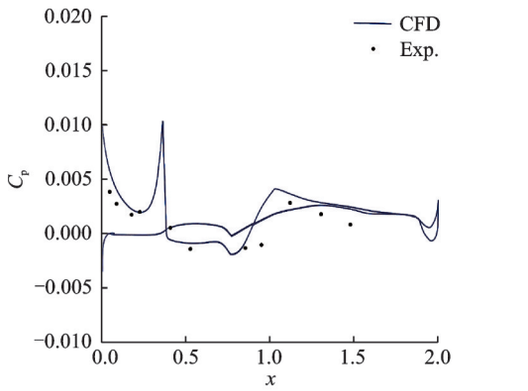

(a) Time-averaged distribution along the fuselage center line

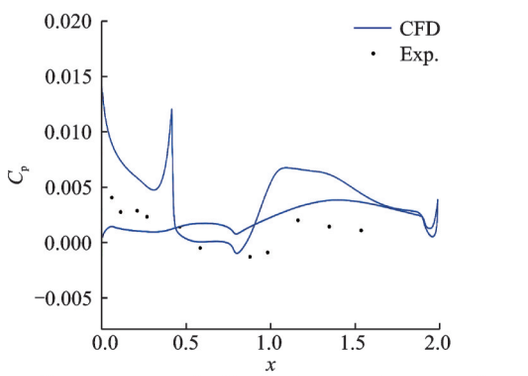

(b) Instantaneous distribution along fuselage center line for an azimuthal angle ψ=0°

Fig.6 ROBIN pressure coefficient distribution comparison with experimental results

benchmark wind tunnel test for this case conducted at the Arnold Engineering Development Center refers to the work in Refs.[30-31]. Table 3 indicates the key parameters of the EGLIN model[32].

Table 3 EGLIN model test parameters[32]

Parameter	Value
Mass/kg	906.87
Store length/mm	3 017.5
Store diameter/mm	500
Center of gravity position/mm	1 417 (from nose)
Fin disposition	Crucifix shape
Forward ejector position/mm	1 237.5 (from nose)
Forward ejector force/kN	10.7
Afterward ejector position/mm	1 746.5 (from nose)
Afterward ejector force/kN	42.7
Ejector length/mm	100

The mesh topology on the geometry can be seen in Fig.7. The model is composed of two overset mesh subdomains with the main domain that includes the entire flow-field as well as the wing and the pylon and the second domain that is attached to

the store itself. The main domain is composed of 1 490 793 tetrahedral cells and the second domain is composed of 122 599 tetrahedral cells. The simulation was conducted in conformity to the initial test conditions of Heim at a super-sonic speed of Mach 1.2 and for a simulation time of 1 s.

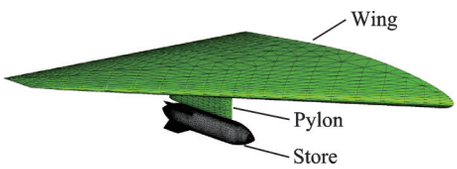

Fig.7 Mesh distribution for the releasing trajectory validation

Fig.8 shows the path of the store for each 0.1 s after the moment it got released from the pylon. Fig.9 compares the position and velocity of the center of gravity (CG) of the store with experimental data[31].

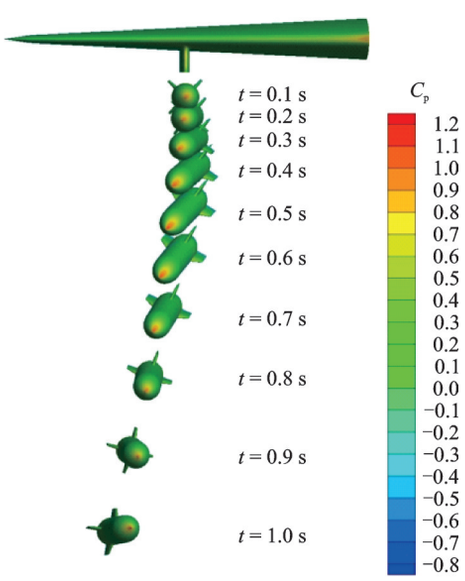

Fig.8 Separation of store at each 0.1 s filled with pressure coefficient contour

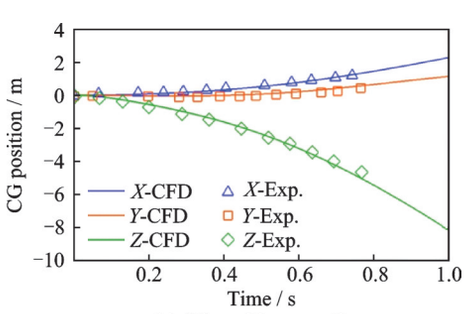

(a) CG position over time

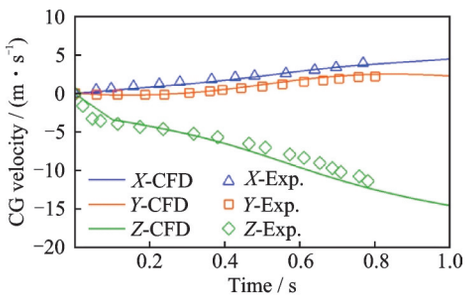

(b) CG velocity over time

Fig.9 Comparison of the dynamic behavior for a dropped store between 6-DOF-CFD solver and experimental data[31]

The graphics show that the CFD-simulated data are consistent well with the experimental ones. This implies good maneuverability and good fidelity of the 6-DOF solver solicitated in Star CCM+.

1.4 Verification

To assess the numerical accuracy and stability of the simulations, a systematic convergence study was performed through progressive grid refinement and reduction of the temporal step size. In a numerically consistent discretization of the governing equations for laminar flow, the computed solution is expected to asymptotically approach a grid-independent value as both spatial and temporal resolutions are increased. Consequently, a grid-convergence assessment was conducted for the Black Hawk helicopter in hovering flight by varying the cell density across the individual sub-meshes and by adjusting the time-step size employed between successive computational iterations. In this study, three cases have been considered and the time averaged lift $\bar{L}$ is acquired. The results are represented in Table 4.

Table 4 Time averaged lift $\bar{L}$ for different mesh resolution

Mesh resolution	$\bar{L}$/N
12 million cells	46 136
9 million cells	47 056
6 million cells	47 152

Taking these findings into account, a computational grid consisting of 9 million cells was selected for further simulations. This resolution demonstrated satisfactory performance, achieving an accept-

able trade-off between computational demand and numerical accuracy, with an estimated deviation of around 2% compared to the most refined mesh. Furthermore, additional simulations were performed with varying time-step sizes, and the corresponding results are reported in Table 5.

Table 5 Time averaged Lift $\bar{L}$ for different time step

Time interval per cycle/s	$\bar{L}$/N
0.000 5	46 348
0.001	46 587
0.01	47 219

Taking these results into account, a temporal resolution of 0.001 s per cycle was selected as an optimal compromise between accuracy and computational cost, yielding an error of approximately 0.5% when compared to finer time steps. The results presented in the table exhibit marginal discrepancies across different temporal and spatial resolutions, indicating that the solution is largely insensitive to discretization refinement. This consistency confirms that the numerical model has attained both spatial and temporal convergence, with residuals and flow parameters stabilizing after approximately three complete rotor revolutions.

2 Results and Discussion

Once the verification is completed and acknowledged, the simulation of the dynamic response of the rocket during release phase has been simulated. The overset mesh flow solver showcased before as well as the 6-DOF equations of motion have been used for simulation under different flight conditions. The model presented previously is composed of seven subdomains, viz., the fuselage, four rotor blades, the far field and the missile. The fuselage block is composed of 2 900 764 polyhedral cells, the far field which is treated as the background mesh is composed of 671 396 polyhedral cells, and each blades block is composed of multiple cells varying from 1 160 356 to 1 155 057 polyhedral cells. Finally, the missile block is composed of 438 023 polyhedral cells. In total, the whole domain is therefore composed of 9 078 503 polyhedral cells and 28 879 975 vertices.

Initially, the simulation is run for three rotor rotations in order for the unsteady flow-field to converge and stabilize. Therefore, the missile is released directly applying a 6-DOF motion, the simulation was continued for three rotor revolutions and the data are extracted to be analyzed. The simulation is run on a workstation equipped with an Intel Xeon 40-core processor and 116 GB of RAM. One rotor revolution takes approximately 12 h to complete in this configuration.

Simulation and results are studied for two different flight regimes: Hovering flight, representing a stationary release and forward flight, with air speeds of 100 km/h and 200 km/h, respectively.

2.1 Hovering flight: Effect of missile launching thrust

Data for missile launching thrust is hard to find freely in achieved documents, thus the thrust chosen for the purpose of this study using the open data[11]. Three thrust values were tested: 5 180, 7 180 and 13 600 N, respectively. For every case, the missile was released from its initial location beneath the rotor with its thrust applied from its nozzle staying consistently along its longitudinal axis.

In Fig.10, different positions of the missile's CG are displayed. The rocket is assumed to be fired at a rotor blade azimuthal angle of 0°. The results show that the trajectory is nominal on the longitudinal axis of the missile with different speeds with the missile leaving the rotor disk area (approximately 9 m) at 0.25, 0.4 and 0.45 s in a croissant order of thrust respectively. For the horizontal position over time, almost no change appears while in the rotor disk area but increase once exiting the rotor disk area. The vertical position over time shows a normal descent of the missile along the whole simulation. The 13 600 N thrust missile sees its descent trajectory stabilized after passing 30 m ahead of the helicopter rotor disk area.

For the rotation, all cases show a change in motion from a pitch down to a pitch up of the missile once passed the close proximity of the helicopter fuselage and before exiting the rotor disk area.

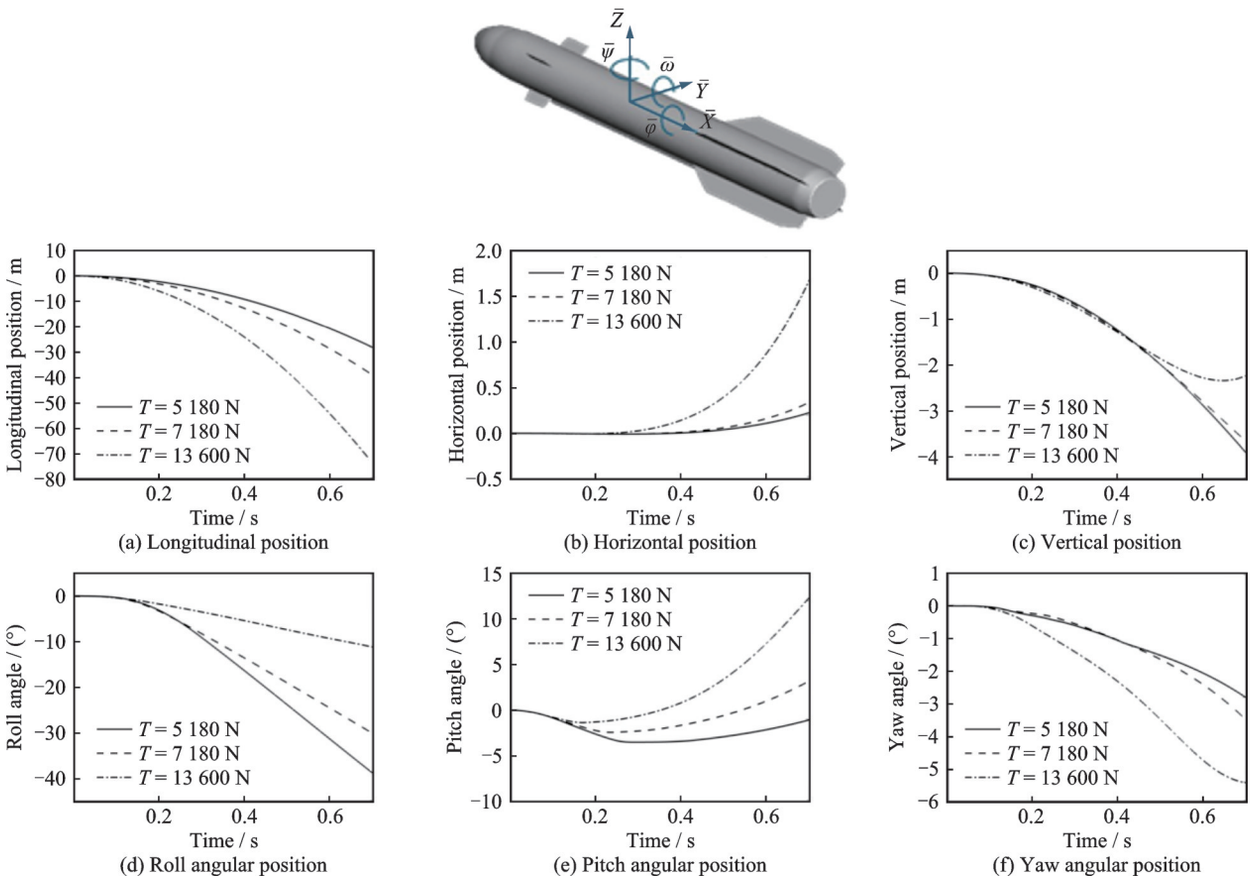

Fig.10 Missile's CG positions over time during release in hovering flight

These changes can be explained by the intervention of the fins attached to the missile that could interact with the unsteady air surrounding the rockets when released.

Fig.11 shows the air vorticity for different planes in the domain near the helicopter and can help to better link the results seen in Fig.10. First, it is possible to see the contained vorticity of the air in the rotor trail in Fig.11(a). The figure shows high vorticity in the close proximity of the end of the trailing edge which is the results of TV created by the blade. As the flow leaves the blade the vorticity decreases showing a high diffusion of the TV in surrounding flow. Thus, in Fig.11(b), the same phenomenal is displayed but in the missile's normal plane. It is possible to see some regions of high vorticity near the edge of the fuselage in this planes, like the wing support of the missile launcher as well as the stabilizer on the right of the tail. At the same time, a circle of turbulent flow can be seen with a

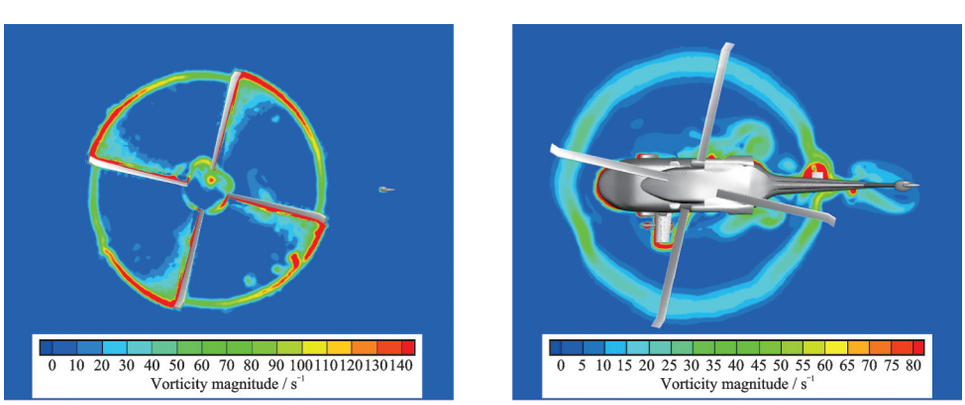

Fig.11 Vorticity magnitude in hovering flight on different planes

size comparable to the rotor disk and result of the downwash flow of the rotor. This turbulent flow will be crossed by the store and impact its trajectory as seen above.

2.2 Forward flight: Effect of helicopter flight speed

In comparison to hovering flight case, forward flights see the helicopter deal with the incoming flowfield generated by its relative motion with the ambient air and depending on its air speed. Simulations were performed for a launching thrust at 7 180 N and for two different helicopter forward flight speeds at 100 and 200 km/h, respectively. Afterwards, the data will be compared with the hovering case of the same launching thrust.

Fig.12 shows the vorticity of the air in the rotor normal plane and the missile's normal plane for different helicopter air speed. In the figure, it is possible to see the high impact of the surrounding airspeed in the propagation of the vorticity as well as the impact of the rotation of the blade in the TV creation.

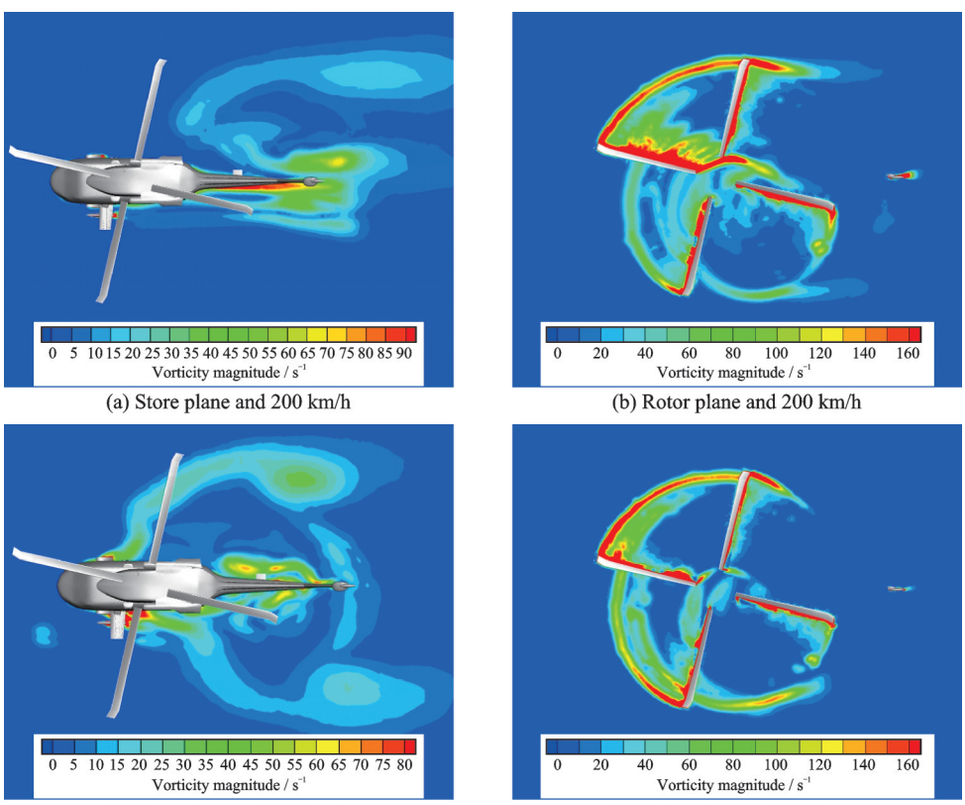

(a) Store plane and 200 km/h (b) Rotor plane and 200 km/h

(c) Store plane and 100 km/h (d) Rotor plane and 100 km/h

Fig.12 Vorticity magnitude in forward flight on different planes and for different airspeeds

Indeed, for the 100 km/h case, the turbulent air will be stronger and more present around the advancing blade than around the retracting blade. At the same time, the vortices are flowing along the flow direction in comparison of the hover case where it was confined in the rotor disk area. The same phenomenon can be seen for the 200 km/h case with stronger amplitude and characteristics. This behavior of the air then does not have any impact on the nose of the helicopter as seen in Fig.12(a) and Fig.12(c), where the air in the missile's normal plane does not present high vorticity.

Fig.13 shows the different positions of the missile's CG over time. As for the hovering flight, the rocket is assumed to be fired in the same conditions. The longitudinal position evolution does not show any significant change, meaning no clear impact of the flow field. The vertical position changes lightly between the different speeds with the slowest drop rate being for the 100 km/h cases. This change is

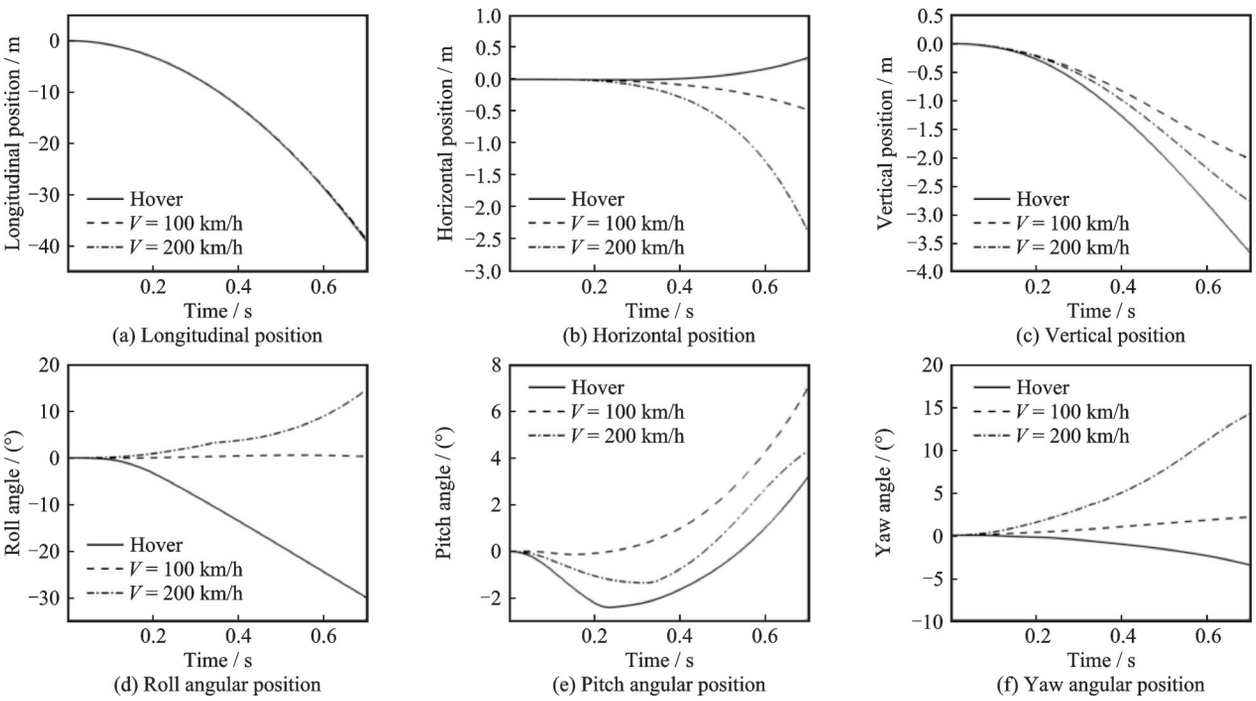

Fig.13 Missile's CG positions over time during release in forward flight

possibly due to the extra lift generated by the fins when in motion with the high velocity flow field surrounding it. For the horizontal position, the different cases produce different results but lead to a left yaw of the missile in comparison to the right yaw observed before in the hovering cases. Angular position evolution shows difference of behavior between the cases. Indeed, every case got different results with no predictable link within each of them. Thus, there will be a high pitch down movement in the hovering case before reverting to pitch up as soon as it exits the rotor disk area. For yaw and roll, there will be almost no changes in the 100 km/h case, resulting in a lower vertical drop. The 200 km/h case will exhibit light roll, pitch up and yaw movement, which results in a higher dropping.

2.3 Comparison of the two configurations

In the first time, the change in acceleration of the missile in three directions was plotted from the case studied before, as shown in Fig.14. It is possible to observe that the missile behaves in an uncontrolled way with numerous and quick change in the acceleration trend of the missile across those three directions. Therefore, the missile seems to get to a point of equilibrium and thus does not exhibit sporadic change in its movement.

In addition to these figures, and to acknowledge the choice of simulating the missile on only one side of the helicopter, the airspeed on the X direction is plotted for the three different cases.

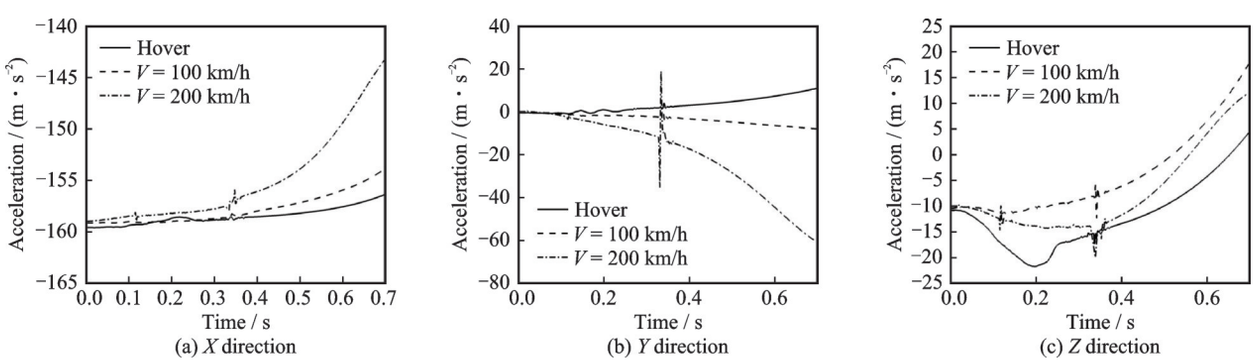

Fig.14 Acceleration of the missile in the three dimensions for the different test cases

Fig.15 depicts the air velocity variation along the flow direction (X direction). In the hovering condition, the relative velocity difference between the two sides of the helicopter is nearly negligible, indicating a largely symmetric airflow distribution. Although the presence of the mounted wing induces localized disturbances beneath both the wing and the missile plane, its overall impact on the global flow field remains minor. However, under forward flight conditions, the velocity asymmetry becomes more evident. For the 100 and 200 km/h cases, a relative velocity difference of approximately 5 m/s is observed, corresponding to about 18% and 9%, respectively. These findings underscore the disparity between the advancing and retreating rotor sides, while also revealing that the wing mounted on the left side modifies the flow distribution and perturbs the natural development of turbulence.

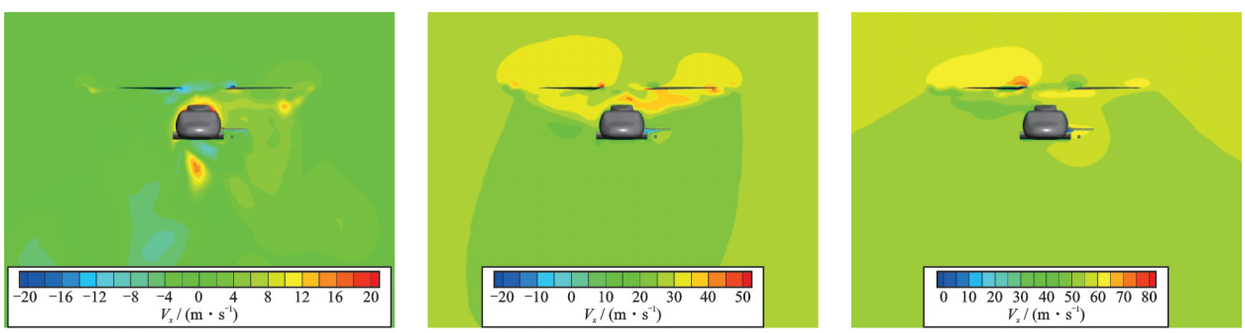

(a) V_x for the hovering case

(b) V_x for the forward case with a speed of 100 km/h

(c) V_x for the forward case with a speed of 200 km/h

Fig.15 Air velocity on the X direction for the different test cases

3 Conclusions

Extensive numerical simulations of the unsteady flowfields around a helicopter configuration were conducted to investigate the impact of the main rotor downwash on a missile launched from it. To this extent, STAR CCM+ URANS solver as well as 6-DOF solver have been used in addition to an unstructured overset mesh grid. The situation has been tested out for different flight and operation conditions. For the studied helicopter model, the tail rotor and the detail structures of the missile pylon are neglected due to their slight effect on the overall flow simulation, however, this is still worthy to be analyzed to clearly identify their effect on the release behavior of the missile.

Simulation results showed that the effect of the downwash generated from the main rotor is more present in hovering flight conditions, as the flow is directed downward and thus creates high air-vorticity. For hovering flight scenario, varying launch thrust of the missile is able to literately change its trajectory and thus shows a direct impact of the downwash in the missile dynamics, as the high-thrusted missiles exhibit less modification in their path in comparison of the low-thrusted ones. For the forward flight case, the rotor wake flow interacts with the surrounding flow and naturally moves backward of the helicopter. In this configuration, the missile trajectory is less impacted by the rotor wake, but needs to face new aerodynamic parameters as the lift and drag created by the body and the fins of it.

The model and simulation in this paper present certain limitations. The current model uses store geometry that has not been extensively tested, and will result in nullified results and impact the simulation. At the same time, the study only uses missiles on its left side for low-computation cost. Since the tip vortices generated by the advancing and retracting tend to increase and decrease respectively as the helicopter's relative airspeed increases, the results will be different for the right side. Thus, it could be interesting to continue the simulation with missiles positioned on both sides of the helicopter and compare the end results.

References

[1] PETRESCU R V, AVERSA R, AKASH B, et al. About helicopters[J]. Journal of Aircraft and Spacecraft Technology, 2017, 1(3): 204-223.

[2] CONLISK A T. Modern helicopter rotor aerodynamics[J]. Progress in Aerospace Science, 2001, 37(5): 419-476.

[3] GONZALEZ A R, CIFUENTES M J, GELVEZ E A. Computational investigation of the effects of rotor wake on helicopter aerodynamics[J]. Journal of Aircraft, 2019, 56(4): 1483-1498.

[4] REICH D B, ELBING B R, BEREZIN C R, et al. Water tunnel flow diagnostics of wake structures downstream of a model helicopter rotor hub[J]. Journal of the American Helicopter Society, 2014, 59(3): 1-12.

[5] LEISHMAN J G. Principles of helicopter aerodynamics[M]. Cambridge: Cambridge University Press, 2006.

[6] LI G Z, CAO T G. Numerical simulation of the wake generated by a helicopter rotor in icing conditions[J]. Fluid Dynamics and Materials Processing, 2021, 17(2): 235-252.

[7] SHANKS S, AHMAD J. Aerodynamics of powered missile separation from a wing[C]//Proceedings of the 22nd Fluid Dynamics, Plasma Dynamics and Lasers Conference. Honolulu: AIAA, 1991: 1663.

[8] CAVALLO P, SINHA N, FELDMAN G. Parallel unstructured mesh adaptation for transient moving body and aeropropulsive applications[C]//Proceedings of the 42nd AIAA Aerospace Science Meeting and Exhibits. Reno: AIAA, 2004: 1057.

[9] TAYLOR R B, LANDGREBE A J. Investigation of the airflow at rocket trajectory and wind sensor locations of a model helicopter simulating low speed flight: UTRC Contract Report, R79-9129855[R]. [S.l.]: [s.n.], 1979.

[10] WEI F S, GJESTVANG J. Store separation analysis of the Penguin missile from the SH-2G helicopter[C]//Proceedings of the 39th AIAA Aerospace Science Meeting and Exhibits. Reno: AIAA, 2001: 992.

[11] LEE B S, CHOI J H, KWON O J. Numerical simulation of free-flight rockets air-launched from a helicopter[J]. Journal of Aircraft, 2011, 48(5): 1766-1775.

[12] ZHOU W Y, YANG G Q, GAO X, et al. Numerical simulation of missile air-launched dynamic process under downwash flow of helicopter rotor[C]//Proceedings of the 33rd Congress of the International Council of the Aeronautical Sciences. Stockholm:[s.n.], 2022: 992.

[13] GONG H, KWAK E, LEE S, et al. Prediction of trajectories of projectiles launched from helicopters[J]. Journal of the Korean Society for Aeronautical & Space Sciences, 2014, 42(3): 213-220.

[14] CROZON C, STEIJL R, BARAKOS G N. Numerical study of helicopter rotors in a ship airwake[J]. Journal of Aircraft, 2014, 51(6): 1813-1832.

[15] WADCOCK A J, EWING L A, SOLIS E, et al. Rotorcraft downwash flow field study to understand the aerodynamics of helicopter brownout[M]. [S.l.]: NASA Ames Research Center, 2008.

[16] OKAMOTO K, DUGUE E P N, AHMAD J, et al. Numerical simulations of an unsteady rocket launch from the AH-64D Apache Longbow helicopter[C]//Proceedings of the 4th Symposium on Overset Composite Grid and Solution Technology. Aberdeen:[s.n.], 1998.

[17] RYU M, SHIN P, LEE T, et al. Aerodynamic analysis of store jettison on a helicopter[C]//Proceedings of the 45th European Rotorcraft Forum. Warsaw: [s.n.], 2019.

[18] TOTAH J. A critical assessment of UH-60 main rotor blade airfoil data[C]//Proceedings of the 11th Applied Aerodynamics Conference. Monterey: AIAA, 1993: 105.

[19] Missile Defense Project. Hellfire, missile threat, center for strategic and international studies[EB/OL]. (2020-05-04) [2025-06-09]. https://missilethreat.csis.org/missile/agm-114-hellfire/.

[20] STEGER J L, DOUGHERTY F C, BENEK J A. A chimera grid scheme[C]//Proceedings of the Legacy CDMS. [S.l.]: AIAA, 1983.

[21] LEMAIRE S. An efficient and accurate overset grid technique applied to maritime CFD[D]. Southampton: University of Southampton, 2023.

[22] NAKAHASI K, TOGASHI F, SHAROV D. Inter-grid-boundary definition method for overset unstructured grid approach[J]. AIAA Journal, 2000, 38(11): 2077-2084.

[23] TOGASHI F, ITO Y, NAKAHASI K, et al. Overset unstructured grids method for viscous flow computations[J]. AIAA Journal, 2006, 44(7): 1617-1623.

[24] MEAKIN R. A new method for establishing intergrid communication among systems of overset grids[C]//Proceedings of the 10th Computational Fluid Dynamics Conference. Honolulu: AIAA, 1991: 1586.

[25] MENTER F R. Improved two-equation k-omega turbulence models for aerodynamics flows: NASA TM 103975[R]. [S.l.]: [s.n.], 1992.

[26] MENTER F R. Two-equation eddy-viscosity turbulence models for engineering applications[J]. AIAA Journal, 1994, 32(8): 1598-1605.

[27] RAYMOND E M, GORTON S A. Steady and periodic pressure measurement on a generic helicopter fuselage model in the presence of a rotor: NASA TM 2000-210286[R]. [S.l.]: [s.n.], 2000.

[28] KENYON A R, BROWN R E. Wake dynamics and rotor-fuselage aerodynamic interactions[C]//Proceedings of American Helicopter Society the 63rd Annual

Forum. Virginia Beach: American Helicopter Society, 2007: 945-962.

[29] ELLIOT J W, ALTHOFF S L, SAILEY R H. Inflow measurement made with a laser velocimeter on a helicopter model in forward flight, Volume 1: Rectangular planform blades at an advance ratio of 0.15: NASA TM 100541[R]. [S.l.]: [s.n.], 1988.

[30] HEIM E R. CFD wing/pylon/finned store mutual interference wind tunnel experiment: AEDC-TSR-91-P4[R]. [S.l.]: [s.n.], 1991.

[31] LIJEWSKI L E, SUHS N E. Time accurate computational fluid dynamics approach to transonic store separation trajectory prediction[J]. Journal of Aircraft, 1994, 31(4): 886-891.

[32] PANAGIOTOPOULOS E E, KYPARISSIS S D. CFD transonic store separation trajectory predictions with comparison to wind tunnel investigations[J]. International Journal of Engineering, 2010, 3(6): 538-553.

Acknowledgements This work was supported by the National Natural Science Foundation of China (No.11602200). The authors would like to acknowledge the following individuals for their assistance: XIAO Tianhang, ZHI Haolin, ZHU Zhenhao, XIAO Jiliang, ZHENG Li, LIN Yinnan and CHEN Meili, all affiliated with the Nanjing University of Aeronautics and Astronautics (NUAA).

Authors

The first author Mr. **COSTERG Fabien** is currently undergoing a double master's degree between National Engineering School of Metz (ENIM) in France and NUAA in China. The first master from ENIM is related to mechanical and industrial engineering with core study like mechanics, fluids mechanics, material science as well as introduction to machining, welding or non-destructive testing. In NUAA, the master's degree is related to aeronautics science and technology and focuses mainly on helicopter rotor dynamics and aerodynamics.

The corresponding author Dr. **DENG Shuanghou** received the B.S. degree in mechanical engineering from Northwestern Polytechnical University, Xi'an, China in 2009, and his M.Sc degree in aircraft design from NUAA in 2012. From 2012 to 2016, he obtained the Ph.D. degree in aerodynamics from Delft University of Technology, the Netherlands. Currently, he is an associate professor in College of Aerospace Engineering, NUAA. His research focuses on aircraft design, aerodynamic configuration of aircraft design and computational fluid dynamics.

Author contributions Mr. **COSTERG Fabien** designed the study, complied the models, conducted the analysis, interpreted the results, and wrote the manuscript. Dr. **DENG Shuanghou** contributed to the discussion and background of the study. Mr. **QIAO Hongyu** supported the simulation and visualization of the present study. All authors commented on the manuscript draft and approved the submission.

Competing interests The authors declare no competing interests.

(Production Editor: ZHANG Huangqun)

直升机下洗流影响下的武器投放特性研究

COSTERG Fabien, 邓双厚, 乔红宇

(南京航空航天大学航空学院,南京 210016,中国)

摘要: 直升机机载武器发射投放过程的姿态和轨迹与高速旋转主旋翼强烈下洗流存在较为强烈的动态耦合特性,从而影响武器投放的安全性和精准性。本文以UH-60通用直升机和AGM-114地狱火导弹为对象,利用高精度数值仿真方法研究直升机下洗流影响下的武器投放特性。数值方法采用非定常雷诺平均Navier-Stokes(Unsteady Reynolds-averaged Navier-Stokes,URANS)结合6自由度(Six-degree-of-freedom,6-DOF)的气动-运动耦合仿真方法,结合嵌套网格技术对直升机悬停和前飞情况下武器投放全过程开展动态仿真。数值仿真结果表明,在悬停状态下,武器投放的稳定性受到直升机主翼下洗流的影响较为明显;随着前飞速度的增加,下洗流和导弹运动特性的耦合影响降低,但会带来轴向不对称的特性从而影响导弹的横航向轨迹。研究结果可为直升机机载武器的投放策略提供参考。

关键词: 直升机旋翼尾流;下洗效应;6-DOF模型;非定常雷诺平均Navier-Stokes(URANS);释放问题

研究亮点:

1. 针对直升机和其挂载的机载武器系统建立了CFD-6-DOF的气动-运动耦合求解方式,可更为准确地预示武器投放的动力学特性。

2. 分别开展了悬停和前飞状态不同下洗流强度下武器投放的动力学特性研究,可更为全面地评估多工况下的投放特性。